RF Tomography of Metallic Objects in Free Space: Preliminary Results

Jia Li[a], Robert L. Ewing[b], Charles Berdanier[b], Christopher Baker[c]
[a]Dept. of Electrical and Computer Engineering, Oakland University, Rochester, MI USA 48309;
[b]Sensors Directorate, Air Force Research Laboratory, WPAFB, OH USA 45433;
[c]Dept. of Electrical and Computer Engineering, Ohio State University, Columbus, OH USA 43210

ABSTRACT

RF tomography has great potential in defense and homeland security applications. A distributed sensing research facility is under development at Air Force Research Lab. To develop a RF tomographic imaging system for the facility, preliminary experiments have been performed in an indoor range with 12 radar sensors distributed on a circle of 3m radius. Ultra-wideband pulses are used to illuminate single and multiple metallic targets. The echoes received by distributed sensors were processed and combined for tomography reconstruction. Traditional matched filter algorithm and truncated singular value decomposition (SVD) algorithm are compared in terms of their complexity, accuracy, and suitability for distributed processing. A new algorithm is proposed for shape reconstruction, which jointly estimates the object boundary and scatter points on the waveform's propagation path. The results show that the new algorithm allows accurate reconstruction of object shape, which is not available through the matched filter and truncated SVD algorithms.

Keywords: RF tomography, ultra-wideband, distributed sensing, shape reconstruction, iterative reconstruction, radar imaging

1. INTRODUCTION

Due to its capability to fuse spatial and frequency diversity, radio frequency (RF) tomography has been studied in the past decades for different applications. For example, Wicks etc. proposed narrow band tomographic radar to track moving targets for security and surveillance [1]. Lo Monte etc. used RF tomography for underground imaging [2-3]. Hamilton etc. proposed propagation models for non-cooperative localization using wireless sensor network tomography [4]. In medical community, Gilmore etc. prototyped an ultra-wideband tomographic imaging system for soft-tissue imaging [5]. Generally speaking, RF tomography is an inverse scattering problem. The analogy between RF tomography and computed tomography in medical domain was recognized long time ago [6-9]. The existing RF tomography systems can be classified into two categories according to the techniques used [10]. The first category is based on radar techniques with applications in localization and target tracking [1, 4, 11-14]. The second category is based on tomographic techniques aimed at reconstruction of parameters of a region of interest [2-3, 5, 15-16]. Most systems in the first category enjoy computationally efficient time-domain algorithms, while systems in the second category usually employ iterative inversion algorithms. The experiments and simulation setup described in this paper fall into the first category. However, our interests in exploring the capability of shape reconstruction leads to an iterative algorithm, which jointly estimates the scatter points on waveform propagation path and object boundary.

The existing RF tomography imaging systems are mostly narrowband or multifrequency. The reconstruction results of such kind of systems are sensitive to the operating frequency because the illuminating fields may interact with the object and excite resonance. When ultra-wideband (UWB) pulse is used in operation, the concern of resonant character is greatly reduced. UWB pulse can also provides very high range resolution, which makes accurate shape reconstruction a more achievable task. In our experiments, we have adopted UWB pulse to illuminate metallic objects with an intention to reconstruct boundary profile of the objects. Due to its role in target recognition, shape reconstruction is an important topic in RF imaging [17-23]. The developed methods include Kirchhoff approximation [17-19], iterative inverse scattering approach [22], and point source method [23]. The objects in consideration are usually perfect conductors or

Radar Sensor Technology XIX; and Active and Passive Signatures VI, edited by G. Charmaine Gilbreath
Kenneth I. Ranney, Chadwick Todd Hawley, Armin Doerry, Proc. of SPIE Vol. 9461, 94610S

metallic. Our method is based on physical optics or Kirchhoff approximation. When scatters surface is flat relative to the impinging wavelength and not interacting, physical optics model is a fairly accurate approximation. With a multistatic circular geometry setup, UWB pulse's time of arrival for each Tx/Rx pair contains the information of scatter location. However, all the points on the elliptical locus formed by the Tx/Rx pair and the distance derived from time of arrival are potential solutions for the scatter location. Equipped with reasonable amount of distributed sensors, we solve the shape reconstruction problem through a joint estimation of scatter locations and object boundary. This paper is organized as follows. Section 2 describes the multistatic geometric setup of the imaging system, followed by the discussion of reconstruction algorithms in Section 3. The experimental and simulation results are presented in Section 4. Section 5 concludes the paper with future research directions

2. SYSTEM SETUP

2.1 Multistatic geometry

RF tomography imaging systems usually have a multistatic geometry setup. The radar sensors are located on a circle or a closed curve, and can beam at different directions as necessary. Each sensor serves either as a transmitter, a receiver or both. The transmitted waveforms can be single frequency, multi-frequency, or broadband. The spatial diversity of distributed sensors enables a 360 degree view of the scene through sensor information fusion. While the general goal is to reconstruct the spatial and electrical properties of a specific region of interest, we are more focused on the reconstruction of object boundary.

2.2 Sensor distribution

A distributed sensing research facility is being developed in Air Force Research Lab (AFRL). Figure 1 shows an aerial view of the facility. It's composed of 12 radar sensors located on a circle of 100m radius. Each sensor is mounted on a tower and elevated 15.24m above the ground. The sensor is capable to transmit arbitrary waveforms between 200MHz and 1GHz. The expected usages include the generation of complex EM environment, RF tomography, noise radar imaging, hybrid sensor imaging and distributed sensing.

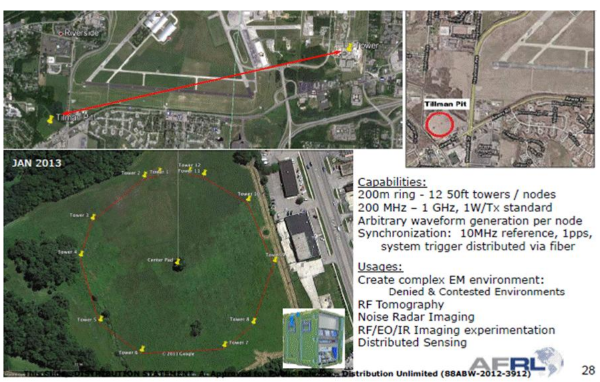

Figure 1 Distributed sensing facility in AFRL.

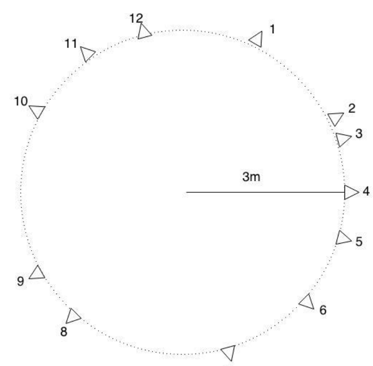

Figure 2 Sensor distribution in the indoor range.

As the distributed sensing research facility is still under development, experiments with the same set up scaled down to a 3m circle have been performed in an indoor range of AFRL. The non-uniform sensor distribution is shown in Figure 2. Each node is a 2-18GHz quad-ridged horn antenna. Sensor nodes are connected a vector network analyzer (VNA) and a digital oscilloscope through ultra-wideband cable. UWB pulse of 10GHz is synthesized by VNA to illuminate spherical metallic objects in the scene.

2.3 Simulation

To validate the reconstruction algorithm and explore how sampling impacts shape reconstruction accuracy, numerical simulations have been performed for different number of sensors uniformly distributed on a circle. The echoes are simulated through a time delay of the UWB pulse corresponding to the length of the propagation path.

3. RECONSTRUCTION ALGORITHMS

RF tomography reconstruction algorithms are discussed in this section. Two traditional reconstruction algorithms, including matched filter processing and truncated SVD algorithms, are discussed first. Based on the characteristic of reflection tomography, an iterative expectation maximization algorithm is proposed for shape reconstruction.

3.1 Truncated SVD

For a bistatic transmitter/receiver pair, let x_{TX} and x_{RX} represent the locations of the transmitter and receiver, separately. For an isotropic point scatter located at x, the time delay associated with the path (x_{TX}, x, x_{RX}) is $t_d = (|x_{TX} - x| + |x - x_{RX}|)/c$, where c is the speed of light. Let $p(t)$ represent the transmitted UWB pulse. Assuming delta function as impulse response, the received waveform can be written as

$$r(t) = ap(t - t_d)e^{j2\pi\theta} + n(t) \tag{1}$$

where a is the attenuation coefficient affected by the reflectivity of the scatter and the distances $|x_{TX} - x|$ and $|x - x_{RX}|$, θ is a random phase, and $n(t)$ is the additive noise. Writing this equation for N pixels in the reconstruction image and discretizing waveforms in vector format will lead to a set of system equations,

$$\boldsymbol{r} = \boldsymbol{P}\boldsymbol{a} + \boldsymbol{n} \tag{2}$$

where $\boldsymbol{r}$ is a $M \times 1$ vector representing the sum of echoes from all the scatters, $\boldsymbol{P}$ is a $M \times N$ matrix with the delayed pulse corresponding to each pixel's location stored in column, $\boldsymbol{a}$ is a $N \times 1$ vector of the unknown attenuation coefficients, and $\boldsymbol{n}$ is the noise vector. This inverse problem can be solved through different techniques. An efficient way to invert the matrix $\boldsymbol{P}$ is through singular value decomposition (SVD). The obtained singular values are usually put in descending order. Small singular values are associated with the directions prone to noise. A threshold can be applied to the singular values to cutoff the contributions from these directions, which is usually referred as truncated SVD method.

Truncated SVD algorithm is a tomographic approach with a fairly high computational complexity of $O(N^3)$. The costly inversion can be done offline so that tomography reconstruction can be performed in real time by multiplying the stored inverse of $\boldsymbol{P}$ with the received waveform. The simplicity makes it suitable for parallel processing in a multistatic setup. The number of pixels N that can be handled by a node's FPGA will determine the image resolution.

3.2 Matched filter

Matched filter, or back projection, is a traditional reconstruction algorithm in radar processing [1]. When solving Eqn. (2), the attenuation vector $\boldsymbol{a}$ can be estimated through,

$$\hat{\boldsymbol{a}} = \boldsymbol{P}^H\boldsymbol{r} = \boldsymbol{P}^H\boldsymbol{P}\boldsymbol{a} + \boldsymbol{P}^H\boldsymbol{n}, \tag{3}$$

as long as the dynamic range of singular values of $\boldsymbol{P}$ is limited. The estimation can be regarded as a convolution between the true attenuation $\boldsymbol{a}$ and a point spread function (PSF) $\boldsymbol{P}^H\boldsymbol{P}$. The footprint of PSF depends on the transmitted waveform as well as the spatial relationship between pixels. Due to the back projection mechanism, the reflectivity of a pixel will spread to the whole elliptical locus formed by the pixel and foci (x_{TX}, x_{Rx}). The width of the stroke is determined by the time duration of the waveform. The longer the pulse duration, the wider the spread in the normal direction of the locus. As UWB pulse is used in our experiment, each scatter will form an ellipse of a narrow stroke in the reconstructed tomography.

3.3 Shape reconstruction through expectation maximization

The extremely high range resolution provided by UWB pulse allows us to explore the possibility of shape reconstruction. The metallic objects in our experiments are impenetrable. It's reasonable to assume the waveform propagation can be approximated through physical optics model because the radii of object surface curvature is much larger than the wavelength and the scatter is not interacting. For an object with convex shape, each bistatic transmitter/receiver pair can illuminate only one scatter point on the metallic object. But the truncated SVD algorithm and back projection cannot distinguish the scatter point from other points on the locus.

Let γ be the closed curve representing an object's boundary and $X = \{x_1, x_2, \cdots, x_K\}$ be the set of scatter points in γ associated with the K Tx/Rx pairs. If the object boundary γ is known, it's easy to calculate the set of scatter points X

from the transmitter and receiver locations. On the other hand, if X is known, γ can be estimated from X. This relationship between γ and X leads us to an expectation maximization (EM) type algorithm for shape reconstruction. The basic idea is to alternately estimate γ and X until convergence. γ is initialized as the boundary of the region confined by the K elliptical loci. Given $\gamma^{(t)}$, find the minimum distance between $\gamma^{(t)}$ and the i-th locus, and the two points associated with this distance. The scatter point $x_i^{(t)}$ is estimated as the middle point of the two points. This combination is to satisfy two regulations. One is the fidelity to the measured time of arrival, while the other is the waveform propagation according to $\gamma^{(t)}$ and (x_{TX}, x_{Rx}). Once $X^{(t)}$ is estimated, $\gamma^{(t+1)}$ is updated through spline fitting to $X^{(t)}$, which provides a smooth curve passing through the scatter points. The pseudo code of the algorithm is given below.

Shape Reconstruction Algorithm

1. $\gamma^{(0)} = \partial\Phi$, where Φ is the region confined by the K elliptical loci reconstructed through matched filtering.
2. For i from 1 to K, do

$$(y_1, y_2) = \arg\min_{y_1 \in \gamma^{(t)}, y_2 \in i\text{th locus}} |y_1 - y_2| .$$

$$x_i^{(t)} = (y_1 + y_2)/2.$$

3. $\gamma^{(t+1)} =$ spline fitting of $X^{(t)}$.
4. Repeat step 2 and 3 if $\left|x_i^{(t)} - x_i^{(t-1)}\right| > \epsilon$ for any i.

4. EXPERIMENTAL AND SIMULATION RESULTS

4.1 Experiments in indoor range

We first present the results of the experiments performed in indoor range. As shown in Figure 2, the 12 radar sensors are distributed on a circle of 3m radius. VNA is used to synthesize 10GHz UWB pulse and quad-ridged horn antenna is used to transmit the pulse. Two metallic objects are present. The first object is a sphere of 12in diameter located at the center of the circle and the same height of radar sensors. The second one is a sphere of 8in diameter located 4ft from the center. Figure 3 shows echoes received by a radar sensor in two scenarios. The upper figure contains the received waveform when the metallic object is presented, while the lower one has no object present. The red asterisks indicate peaks detected. The peak in the lower figure corresponds to the waveform from direct path. It's compared to the peak detection results in the upper figure to remove the clutter. A total of 9 transmitter/receiver pairs were used to obtain the matched filter reconstruction in Figure 4. The location and size of the two objects are clear in the reconstructed image, so is the locus associated with each pair of transmitter and receiver. But the shape of the objects is not reconstructed.

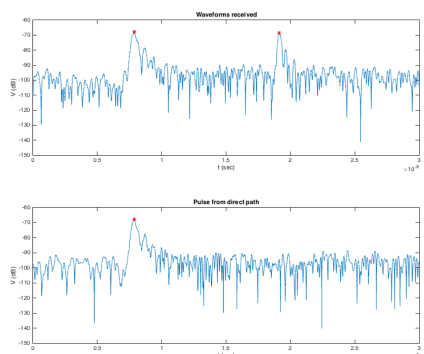

Figure 3 Waveforms received at a sensor node with (upper) and without (lower) target present.

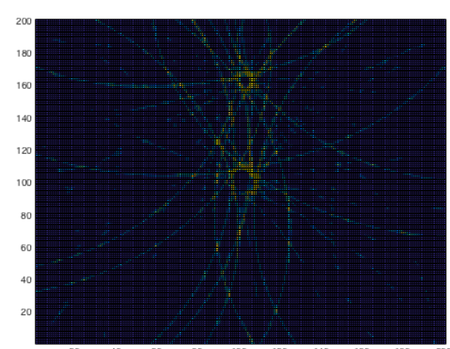

Figure 4 Reconstruction by matched filtering with two metallic objects.

Figure 5 contains the reconstruction results of truncated SVD algorithm. Due to the limit on image size, we have only reconstructed the 2mx2m center region with a 51x51 image. Two subfigures on the left are the reconstruction results of two different Tx/Rx pairs. The subfigure on the right is the combination of the reconstruction of all 9 pairs. Through the comparison of truncated SVD and matched filtering reconstruction, we found that both methods can reconstruct the locus associated with Tx/Rx pair. But the result of truncated SVD is noisier than the matched filter result. Combining with its advantage of low computational complexity, matched filter is clearly a better choice than truncated SVD in the initial tomography reconstruction.

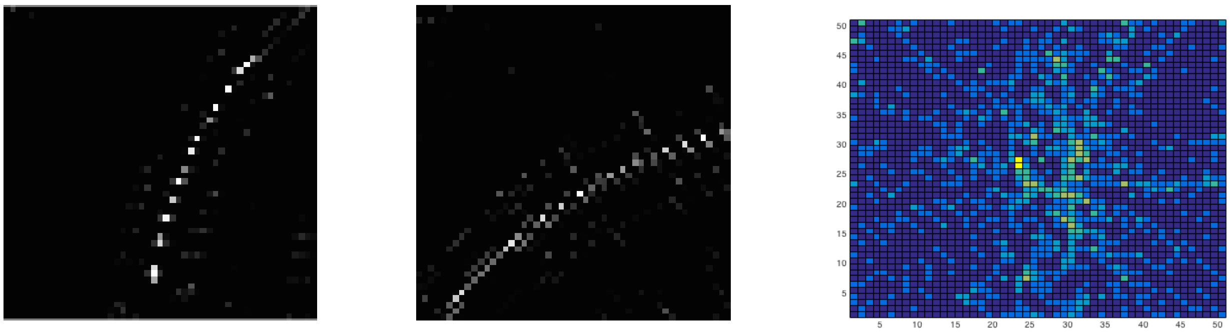

Figure 5 Reconstruction by truncated SVD algorithm.

Using the reconstruction result of matched filter as initialization, the shape reconstruction algorithm usually converges in 5-10 iterations. Figure 6 shows the shape reconstruction result. The blue line shows the true object boundary. The red circles are the estimated scatter points and the green line is the reconstructed object boundary.

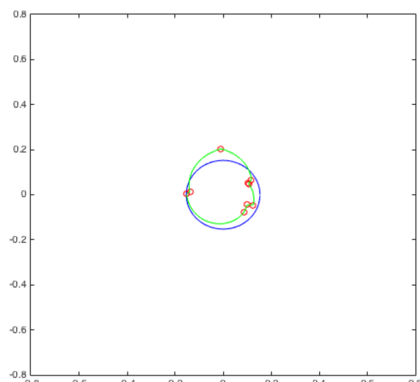

Figure 6 Shape reconstruction result. Blue line: true boundary, red circle: estimated scatter points, green line: reconstructed object boundary.

4.2 Numerical simulations

We are interested in exploring the accuracy of shape reconstruction for different types of shapes and using different number of sensors. Numerical simulation is performed to simulate the scenarios of 12 and 30 Tx/Rx sensors uniformly distributed on a circle of 1.2m radius to reconstruct the boundary of a rectangle and a 2D plane. Figure 7 shows the shape reconstruction results. From left to right, the columns of subfigure are corresponding to the scenario of 1) 12 nodes, rectangle object; 2) 30 nodes, rectangle object; 3) 12 nodes, 2D plane; 4) 30 nodes, 2D plane. And from top to bottom, the rows of subfigure are corresponding to 1) true object boundary and sensor distribution; 2) estimated scatter points; 3) reconstructed object boundary. Even though the sensors are uniformly distributed on the circle, the estimated scatter points are not evenly distributed. The distribution is dense in those protruding points and none or sparse in the concave regions. This is due to the difference in these regions' distance to the Tx/Rx pairs. It can be seen that increasing the number of sensor nodes can improve shape reconstruction accuracy, especially for the case of 2D plane whose concave regions can be better sampled by a larger number of sensors.

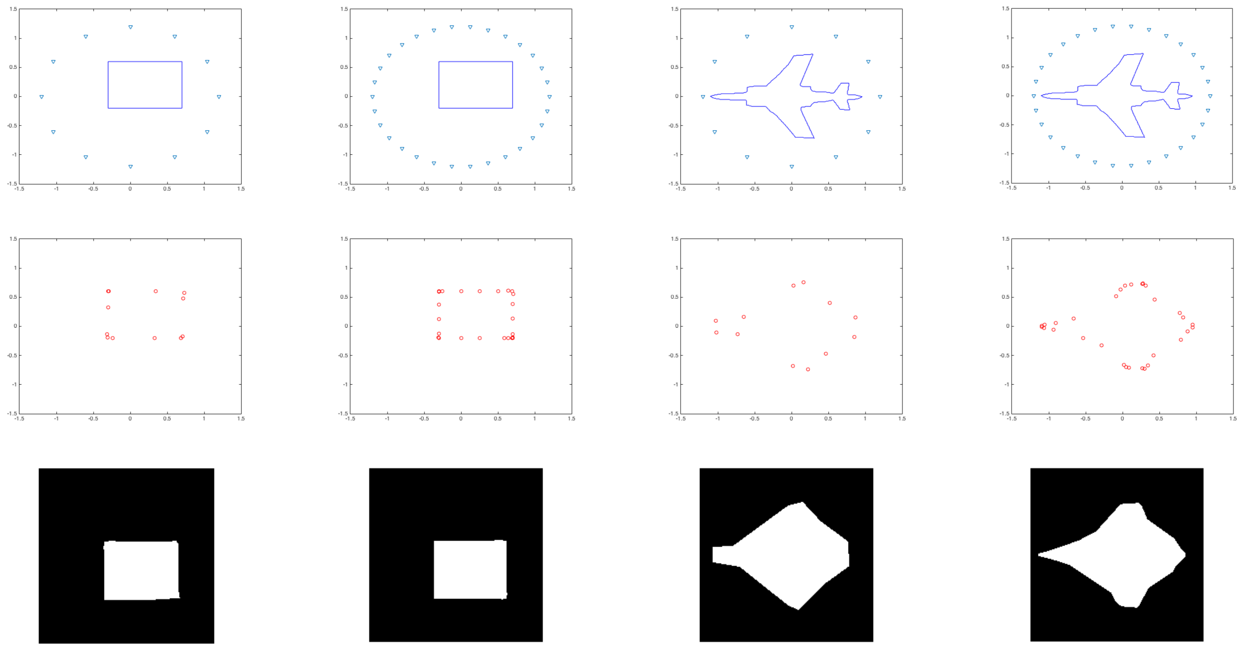

Figure 7 Simulated shape reconstruction results. From left to right: 1) 12 sensors, rectangle; 2) 30 sensors, rectangle; 3) 12 sensors, plane; 4) 30 sensors, plane. From top to bottom: 1) true object boundary and sensor distribution; 2) estimated scatter points; 3) reconstructed object boundary.

5. CONCLUSIONS

We studied the RF tomography of metallic objects in this paper. The traditional truncated SVD method and matched filter method have been applied to tomography reconstruction. It's shown that matched filter method is better than truncated SVD in terms of accuracy and complexity. A new EM type algorithm is introduced to jointly estimate scatter points and reconstruct object boundaries. It's validated by both experimental and numerical simulation results. The current algorithm can reconstruct convex object boundaries very well, but still has difficulty with concave object boundaries. Although only 2D shape reconstruction is studied in this paper, the proposed algorithm can be generated to 3D shape reconstruction by fitting spline surface to the estimated 3D scatter points. After the construction of the distributed sensing research facility in AFRL is completed, these algorithms will be tested with more experiments in the facility, including the use of narrow band pulse and imaging moving targets.

ACKNOWLEDGMENT

This work was performed during Li's visit at Air Force Research Lab, Wright Patterson AFB, OH, in summer 2014. It's supported through National Research Council Research Associateship program. The authors would like to thank Tom Corigliano for his assistance during the experiments.

REFERENCES

[1] Wicks, M. C., Himed, B., Bascom, H. and Clancy, J., "Tomography of Moving Targets (TMT) for Security and Surveillance," Advances in Sensing with Security Applications NATO Security Through Science Series 2, 323-339, (2006).

[2] Lo Monte, L., Erricolo, D., Soldovieri, F. and Wicks, M. C., "Recent Advances in RF Tomography for Underground Imaging," 2010 13th International Conference on Ground Penetrating Radar, 1-6, (2010).

[3] Lo Monte, L., Erricolo, D., Soldovieri, F. and Wicks, M. C., "Radio Frequency Tomography for Tunnel Detection," IEEE Trans. on Geoscience and Remote Sensing 48(3), 1128-1137, (2010).
[4] Hamilton, B. R., Ma, X., Baxley, R. J. and Matechik, S. M., "Propagation Modeling for Radio Frequency Tomography in Wireless Networks," IEEE Journal of Selected Topics in Signal Processing 8(1), 55-65, (2014).
[5] Gilmore, C. Mojabi, P., Zakaria, A., Ostadrahimi, M., Kaye, C., Noghanian, S., Shafai, L., Pistorius, S. and LoVetri, J., "An Ultra-wideband Microwave Tomography System: Preliminary Results," Proc. of 31st Annual International Conference of the IEEE EMBS, 2288-2291 (2009).
[6] Kak, A. C. and Slaney, M., [Principles of Computerized Tomographic Imaging], IEEE Press, New York, (1988).
[7] Norton, S. J. and Linzer, M., "Ultrasonic Reflectivity Imaging in Three Dimensions: Exact Inverse Scattering Solutions for Planar, Cylindrical and Spherical Apertures," IEEE Trans. on Biomedical Engineering, BME-28(2), 202-220, (1981).
[8] Munson, D. C, O'Brien, J. D. and Jenkins, W. K., "A Tomographic Formulation of Spotlight-Mode Synthetic Aperture Radar," Proc. of The IEEE 71(8), 917-925, (1983).
[9] Jakowatz, C. V. and Thompson, P. A., "A New Look at Spotlight Mode Synthetic Aperture Radar as Tomography: Imaging 3-D Targets," IEEE Trans. on Image Processing 4(5), (1995).
[10] Jofre, L., Broquetas, A., Romeu, J., Blanch, S., Toda, A. P., Fabregas, X. and Cardama, A., "UWB Tomographic Radar Imaging of Penetrable and Impenetrable Objects," Proc. of the IEEE 97(2), 451-464 (2009).
[11] Griffiths, H. D. and Baker, C. J., "Fundamentals of Tomography and Radar," Advances in Sensing with Security Applications NATO Security Through Science Series 2, 171-187, (2006).
[12] Parker, J. T., Ferrara, M., Bracken, J. and Himed, B., "Preliminary Experimental Results for RF Tomography Using Distributed Sensing," Proc. of 2010 International Conference on Electromagnetics in Advanced Applications, 549-552, (2010).
[13] Knight, F. K., Kulkarni, S. R., Marino, R. M. and Parker, J. K., "Tomographic Techniques Applied to Laser Radar Reflective Measurements," The Lincoln Laboratory Journal 2(2), 143-160, (1989).
[14] Sego, D. J., Griffiths, H. D. and Wicks, M. C., "Radar Tomography using Doppler-Based Projections," 2011 IEEE Radar Conference, 403-408, (2011).
[15] Geffrin, J. -M., Chaumet, P. C., Eyraud, C., Belkebir, K. and Sabouroux, P., "Electromagnetic three-dimensional reconstruction of targets from free space experimental data," Applied Physics Letters 92, 194103 (2008).
[16] Picco, V., Negishi, T., Nishikata, S., Spitzer, D. and Erricolo, D., "RF Tomography in Free Space: Experimental Validation of the Forward Model and an Inversion Algorithm Based on the Algebraic Reconstruction Technique," International Journal of Antennas and Propagation 2013, 1-9, (2013).
[17] Soldovieri, F., Solimene, R. and Pierri, R., "Reconstructing the contour of metallic planar objects from only intensity scattered field data over a single plane," Optics Express 16(13), 9468–9479, (2008).
[18] Liseno, A., Tartaglione, F. and Soldovieri, F., "Shape reconstruction of 2-D buried objects under a Kirchhoff approximation," IEEE Geoscience and Remote Sensing Letters 1(2), 118-121, (2004).
[19] Pierri, R., Liseno, A., Solimene, R. and Soldovieri, F., "Beyond physical optics SVD shape reconstruction of metallic cylinders," IEEE Transactions on Antennas and Propagation 54(2), 655-665, (2006).
[20] Wildman, R. and Weile, D., "Geometry reconstruction of conducting cylinders using genetic programming," IEEE Transactions on Antennas and Propagation 55(3), 629–636, (2007).
[21] Woten, D., Hajihashemi, M., Hassan, A. and El-Shenawee, M., "Experimental Microwave Validation of Level Set Reconstruction Algorithm," IEEE transactions on antennas and propagation 58(1), 230-233, (2010).
[22] Dorn, O., Miller, E. L. and Rappaport, C. M., "A shape reconstruction method for electromagnetic tomography using adjoint fields and level sets," Inverse Problems 16(5), 1119-1156, (2000).
[23] Potthas, R., "A point-source method for inverse acoustic and electromagnetic obstacle scattering problems," IMA Journal of Applied Mathematics 61, 119-140, (1998).